iScience

CellPress
OPEN ACCESS

Article

Proteasome-mediated degradation of long-range nucleases negatively regulates resection of DNA double-strand breaks

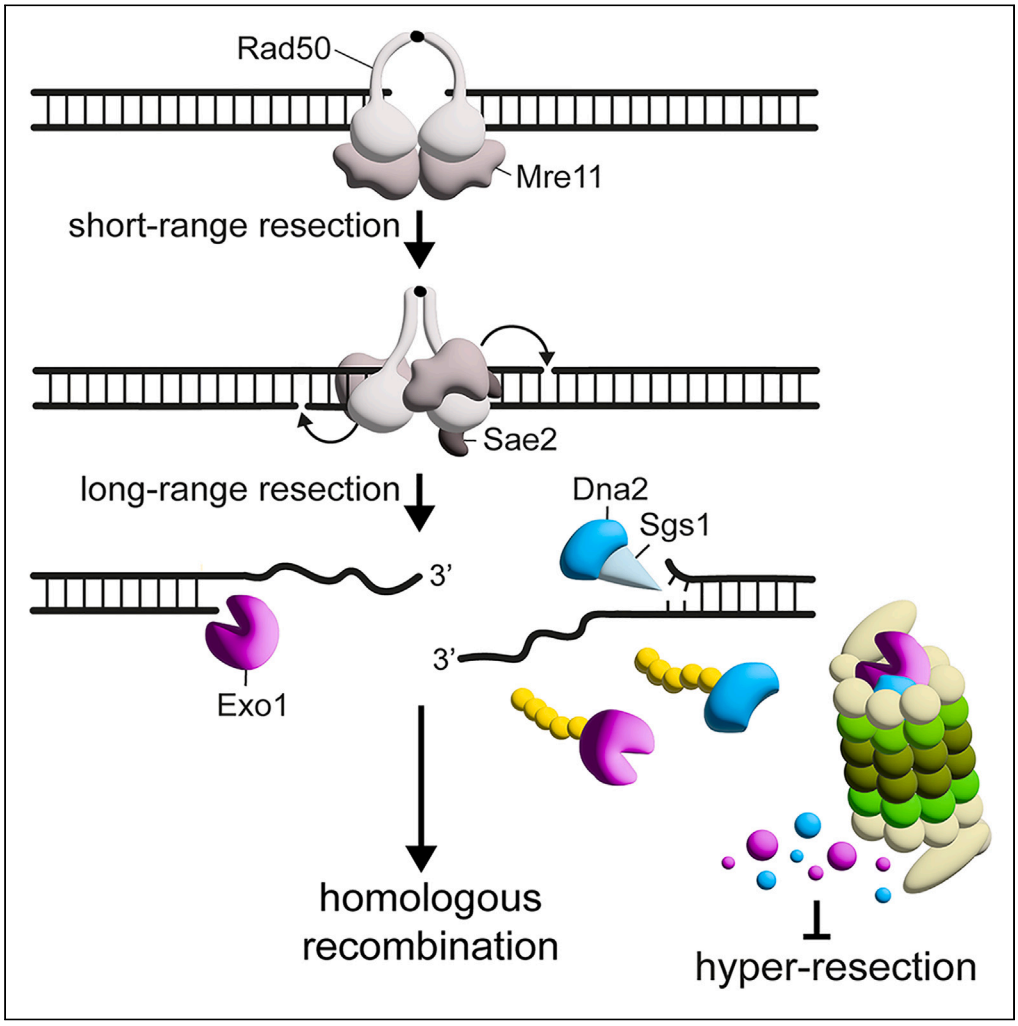

Marco Gnugnoli, Carlo Rinaldi, Erika Casari, Paolo Pizzul, Diego Bonetti, Maria Pia Longhese

mariapia.longhese@unimib.it

Highlights

Proteasome dysfunction leads to hyper-resection

Proteasome dysfunction increases the amount of Exo1 and Dna2 nucleases

Exo1 and Dna2 are ubiquitylated

The proteasome restrains DSB resection by limiting the abundance of Exo1 and Dna2

Gnugnoli et al., iScience 27, 110373
July 19, 2024
https://doi.org/10.1016/j.isci.2024.110373

iScience

CellPress
OPEN ACCESS

Article

Proteasome-mediated degradation of long-range nucleases negatively regulates resection of DNA double-strand breaks

Marco Gnugnoli,[1] Carlo Rinaldi,[1] Erika Casari,[1] Paolo Pizzul,[1] Diego Bonetti,[1] and Maria Pia Longhese[1,2,*]

SUMMARY

Homologous recombination is initiated by the nucleolytic degradation (resection) of DNA double-strand breaks (DSBs). DSB resection is a two-step process. In the short-range step, the MRX (Mre11-Rad50-Xrs2) complex, together with Sae2, incises the 5′-terminated strand at the DSB end and resects back toward the DNA end. Then, the long-range resection nucleases Exo1 and Dna2 further elongate the resected DNA tracts. We found that mutations lowering proteasome functionality bypass the need for Sae2 in DSB resection. In particular, the dysfunction of the proteasome subunit Rpn11 leads to hyper-resection and increases the levels of both Exo1 and Dna2 to such an extent that it allows the bypass of the requirement for either Exo1 or Dna2, but not for both. These observations, along with the finding that Exo1 and Dna2 are ubiquitylated, indicate a role of the proteasome in restraining DSB resection by negatively controlling the abundance of the long-range resection nucleases.

INTRODUCTION

DNA double-strand breaks (DSBs) can be repaired through two primary mechanisms: non-homologous end joining (NHEJ) and homologous recombination (HR). NHEJ allows a direct ligation of the DNA ends with very little or no complementary base pairing, while HR uses an undamaged homologous duplex DNA as a template for repair.[1,2] For HR to occur, the 5′-terminated DNA strands of a DSB must undergo degradation by a concerted action of nucleases in a process termed resection.[3] Resection at the DSB ends generates 3′-ended single-stranded DNA (ssDNA) that serves as a substrate for the recombinase Rad51, allowing homologous pairing and strand invasion.

DNA DSBs also trigger a checkpoint response that is regulated by the apical protein kinases Tel1/ataxia telangiectasia mutated (ATM) and Mec1/ataxia telangiectasia and Rad3-related (ATR), which transmit the checkpoint signal to the effector kinases Rad53/CHK2 and Chk1/CHK1 through the adaptor protein Rad9/53BP1.[4] Tel1/ATM is recruited to DSBs via interaction with the MRX/N (Mre11-Rad50-Xrs2/NBS1) complex, while Mec1 recruitment depends on Ddc2/ATR-interacting protein (ATRIP) association with Replication Protein A (RPA)-coated ssDNA resulting from end resection. Thus, DSB resection also causes a transition from a Tel1- to a Mec1-mediated checkpoint signaling.[5]

In both yeast and mammals, resection of DNA DSBs occurs in two steps. Initially, the Sae2/CtIP protein, upon its phosphorylation by cyclin-dependent kinases (Cdk1 in yeast), promotes the endonuclease activity of Mre11 to incise the 5′-terminated strands on both sides of the DSB.[6] Subsequently, the Mre11 exonuclease resects in a 3′-5′ direction back toward the DNA ends to generate 100–300 nucleotides of ssDNA. Following this initial step, the 5′-3′ exonuclease Exo1/EXO1 and the endonuclease Dna2/DNA2 elongate the resected tracts in the 5′-3′ direction, moving away from the DSB.[7–13] Dna2 acts in conjunction with Sgs1/BLM, whose helicase activity unwinds the double-stranded DNA (dsDNA) to generate a 5′ DNA flap that is cleaved by Dna2.

This Exo1- and Dna2-dependent step, referred to as long-range resection, is essential for processes like interchromosomal HR repair, when the donor allele is located on a different chromosome or on the same chromosome but at a distance greater than 50–100 kb from the DSB.[14–16] Conversely, it is dispensable for DSB-induced HR when a repair template is located in close proximity on the same chromosome,[16] suggesting that MRX-Sae2 generates sufficient ssDNA for Rad51-catalyzed repair.

DSB resection must be tightly regulated to prevent an excessive generation of ssDNA, and this control in *Saccharomyces cerevisiae* is exerted by a complex interplay of regulatory proteins. Firstly, Rad9 limits extensive resection directly by counteracting the activity of Sgs1-Dna2, and indirectly by activating Rad53, which restrains Exo1 activity by phosphorylating its C-terminal regulatory domain.[17–22] Exo1 and Dna2-Sgs1 are negatively regulated also by the Ku70/Ku80 heterodimer, which inhibits Exo1 from binding to DSB ends,[23–27] and by the heterotrimeric 9-1-1 DNA damage clamp (Ddc1-Mec3-Rad17 in yeast), which attenuates the Sgs1-Dna2 pathway by stabilizing Rad9 binding to DSBs.[28] Finally, the Mre11 endonuclease activity is inhibited by the 9-1-1 complex[14] and by the Rif2 (Rap1-Interacting Factor) protein that competes with Sae2 for Rad50 binding.[29,30]

[1]Dipartimento di Biotecnologie e Bioscienze, Università degli Studi di Milano-Bicocca, 20126 Milano, Italy
[2]Lead contact
*Correspondence: mariapia.longhese@unimib.it
https://doi.org/10.1016/j.isci.2024.110373

The lack of Sae2 increases the DNA damage sensitivity and impairs resection of DNA DSBs.[31] Specifically, Sae2 deficiency enhances MRX and Tel1 persistence at DSBs, leading to an increased Rad9 association with DSBs and Rad53 hyperactivation.[17–19,21,32–35] This heightened Rad9 association with DSBs and Rad53 hyperactivation counteract the resection activity of both Sgs1-Dna2 and Exo1, thus explaining the resection defect of *sae2*Δ cells. Furthermore, they are in part responsible for the increased DNA damage sensitivity of *sae2*Δ cells. In fact, reducing Tel1 function, by decreasing either its association with DSBs or its kinase activity, partially suppresses the sensitivity to DNA damage of *sae2*Δ cells.[18] A similar effect is observed when Rad9 is deleted or when Rad53 activity is impaired by reducing either its interaction with Rad9 or its kinase activity.[17–19,21]

In eukaryotes, most proteins are removed via the 26S ubiquitin-proteasome system, a multimeric complex that binds polyubiquitylated proteins and deubiquitylates and unfolds them to allow their degradation.[36] Interestingly, a proteomic analysis of yeast chromatin, before and after DNA damage induced by the radiomimetic drug Zeocin, has revealed alterations in protein composition at sites of DSBs with histones partially removed from chromatin in a proteasome-mediated manner.[37] Furthermore, most components of the proteasome are found to be enriched at sites of DNA damage in yeast,[37,38] and they are part of repair foci in mammalian cells,[39–41] suggesting a proteasome involvement in the degradation of components of the DSB response. Consistent with this hypothesis, treatment with caffeine results in a rapid proteasomal degradation of both Sae2 and Dna2 in yeast cells,[42] whereas Dna2 sumoylation attenuates its nuclease activity and facilitates Dna2 degradation.[43] In humans, EXO1 undergoes ubiquitin-mediated degradation following DSB induction and in response to stalled replication forks. In addition, EXO1 sumoylation was shown to facilitate its ubiquitin-mediated degradation.[44–47]

By searching for extragenic suppressors of the DNA damage sensitivity caused by the lack of Sae2, we found that a reduction in proteasome functionality causes hyper-resection of DNA DSBs and bypasses the need for Sae2 in both DNA damage resistance and DSB resection. This bypass of the Sae2 function is due to an increased amount of the long-range resection nucleases Exo1 and Dna2 that turned out to be ubiquitylated. These findings indicate that proteasome-mediated degradation negatively regulates long-range resection by controlling the levels of Exo1 and Dna2 nucleases.

RESULTS

Mutations in the proteasome subunits suppress the DNA damage sensitivity of *sae2*Δ cells

Sae2 stimulates the endonuclease activity of the MRX complex and negatively regulates the persistence of MRX and Tel1 at DSBs.[6,21,33–35] In cells lacking Sae2, there is an increased MRX and Tel1 association with DSBs, leading to enhanced binding of Rad9 to DSBs. This increased Rad9 association counteracts the resection activity of Sgs1-Dna2[17,19–21] and induces the hyperactivation of Rad53, which in turn leads to the inhibitory phosphorylation of Exo1.[22]

To identify pathways that can bypass Sae2 function in DNA damage resistance and DSB resection, we conducted a genetic screen for mutations that suppress the sensitivity of *sae2*Δ cells to camptothecin (CPT), a compound that stabilizes DNA topoisomerase I cleavage complexes leading to replication-dependent DSBs.[48] The increased DNA damage sensitivity of *sae2*Δ cells is partly attributed to persistent Rad53 activation.[17–19,21,34] To circumvent the identification of mutations that suppress the DNA damage sensitivity of *sae2*Δ cells by merely reducing checkpoint activation, the screening was performed in *sae2*Δ cells that lack also the *RIF2* gene. This approach was based on the finding that the absence of Rif2 reduces Rad53 activation in *sae2*Δ cells to wild-type levels by decreasing the amount of MRX and Tel1 bound at DSBs in these cells.[29] Consequently, *RIF2* deletion partially suppressed the CPT sensitivity of *sae2*Δ cells (Figure 1A).

We isolated 15 CPT-resistant *sae2*Δ *rif2*Δ clones that fell into 7 distinct allelism groups. Through genetic analyses and genome sequencing, we could establish that the suppressing mutations hit the *TOP1* gene, encoding the CPT target topoisomerase I, and the *RPN11*, *RPN5*, *PRE6*, *PRE7*, *PRE8*, and *PRE10* genes, encoding subunits of the 26S proteasome. Each suppressor mutation in the proteasome subunits was due to a single nucleotide substitution except for the *rpn5* allele that carried a stop codon after leucine 412 (Figure 1A). Furthermore, these mutations suppressed the DNA damage sensitivity not only of *sae2*Δ *rif2*Δ but also of *sae2*Δ cells (Figure 1B).

The 26S proteasome is a macromolecular machine that leads to the degradation of protein tagged with a polyubiquitin chain.[49] It is made up of the 20S core particle (CP), which contains the proteolytic active sites and is composed of α-type and β-type subunits arranged in four stacked heptameric rings. This core is capped on one or both ends by a regulatory particle (RP) that comprises two sub-complexes, referred to as the lid and the base, and is responsible for the recognition, unfolding, and transfer of protein substrates into the core.[50] While Pre6, Pre7, Pre8, and Pre10 proteins belong to the CP, Rpn5 and Rpn11 are part of the lid, with Rpn11 possessing a Zn^{2+}-dependent deubiquitylase activity.[51,52]

The identified *RPN* and *PRE* genes are essential for cell viability. The corresponding mutations did not show significant sensitivity to DNA-damaging agents, but all were temperature-sensitive to varying degrees (Figure 1C), suggesting that the corresponding mutant variants reduce proteasome functionality without completely abolishing it. All these mutations completely restored the resistance of *sae2*Δ cells to CPT and methyl methanesulphonate (MMS) (Figure 1B). However, the sensitivity of *sae2*Δ cells to phleomycin was only partially reduced, with the most significant suppression correlating with the highest degree of temperature sensitivity (Figure 1B). This suggests that the mechanism restoring phleomycin resistance differs from the one involved in suppressing CPT and MMS sensitivity.

To assess whether the suppression of *sae2*Δ DNA damage sensitivity is indeed due to impairment of proteasome activity, we introduced the D122A amino acid substitution into the MPN (Mpr1, Pad1 N-terminal) motif of Rpn11. This substitution is known to diminish Rpn11 deubiquitylation activity leading to the accumulation of ubiquitylated proteins.[53] The *rpn11-D122A* allele effectively alleviated the DNA damage sensitivity of *sae2*Δ cells (Figure 1D), indicating that the suppression of *sae2*Δ results from a reduction of proteasome activity.

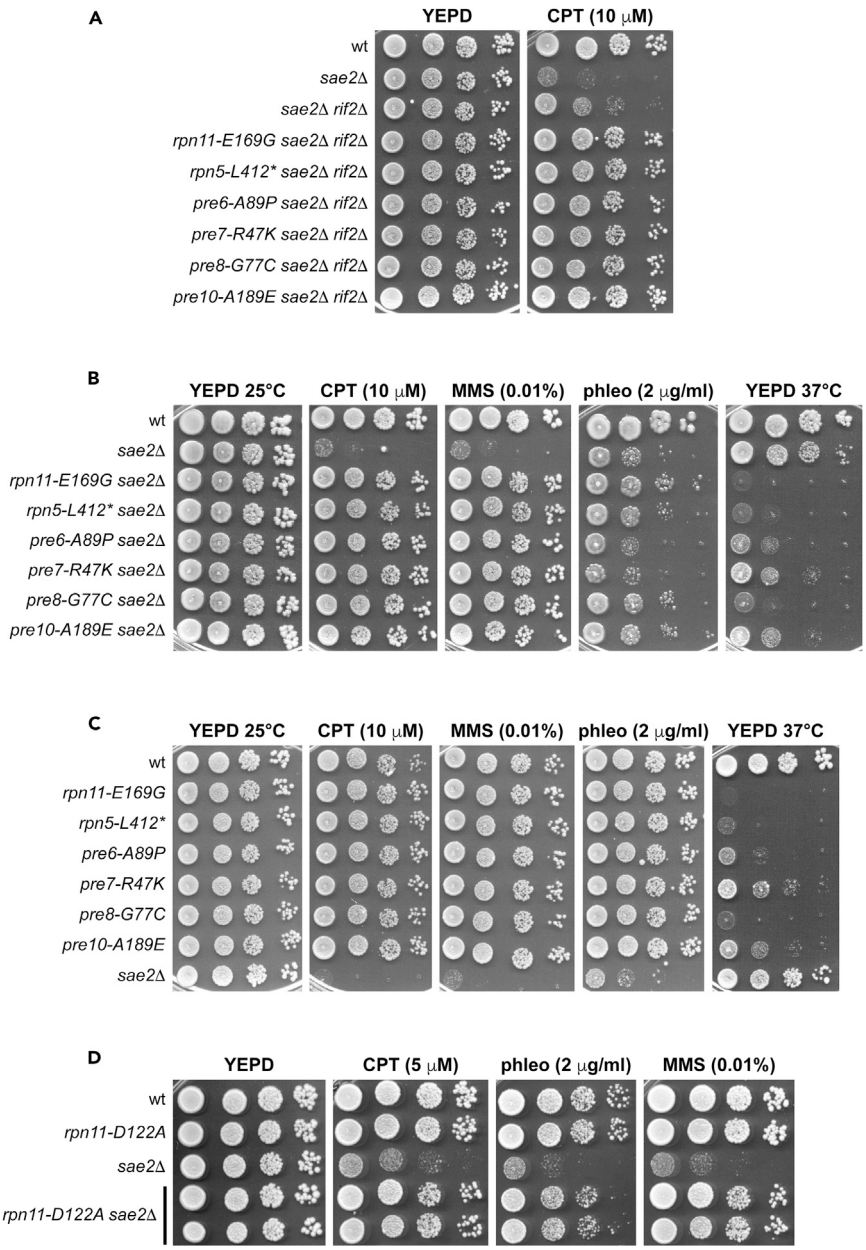

Figure 1. Suppressors of the DNA damage sensitivity of *sae2Δ* cells

(A–D) Exponentially growing cells were serially diluted (1:10), and each dilution was spotted out onto yeast extract peptone dextrose (YEPD) plates that were incubated at 25°C or at 37°C and onto YEPD plates containing CPT, MMS, or phleomycin that were incubated at 25°C.

The *rpn11-E169G* allele suppresses the resection defect of *sae2Δ* cells and increases DSB resection and repair by single-strand annealing

We focused on Rpn11 because its human ortholog, POH1, has been implicated in DSB repair and promotes DSB resection by relieving the resection barrier exerted by the RAP80 protein.[54,55] Moreover, the *rpn11-E169G* allele does not reduce cell viability at 25°C and is one of the most effective in counteracting the sensitivity of *sae2Δ* cells to phleomycin at 25°C (Figure 1B).

We first investigated whether the *rpn11-E169G* mutation suppressed the sensitivity to genotoxic agents of *sae2Δ* cells by restoring DSB resection. We directly monitored ssDNA generation at the DSB ends by introducing the *rpn11-E169G* allele in a haploid JKM139 strain carrying the homothallic (*HO*) gene under the control of a galactose-inducible promoter (*GAL-HO*).[56] In this strain, the addition of galactose induces HO expression, resulting in a single DSB at the *MAT* locus. This DSB cannot be repaired by HR because the homologous donor loci, *HML* and *HMR*, are deleted. Cells exponentially growing in raffinose were shifted to galactose to induce HO expression, and genomic DNA

was analyzed at different time points after HO induction. Since ssDNA is resistant to restriction enzyme cleavage, the 5′-3′ nucleolytic degradation at the DSB ends progressively exposes *Ssp*I sites located at increasing distances from the HO-cut site (Figure 2A), leading to the appearance of slower-migrating bands (r1-r6) detectable by denaturing gel electrophoresis and Southern blot analysis with a single-stranded probe that hybridizes to the unresected strand on one side of the DSB.[57] The appearance of the ssDNA intermediates at the HO-induced DSB was markedly increased in *rpn11-E169G sae2*Δ cells compared to *sae2*Δ cells (Figures 2B and 2C), indicating that *rpn11-E169G* suppresses the resection defect caused by the lack of Sae2.

Sae2, when phosphorylated by Cdk1, stimulates the Mre11 endonuclease activity that catalyzes an incision of the 5′ strand at the DSB ends.[6] Thus, we asked whether the *rpn11-E169G* mutation might circumvent the need for Sae2 in the activation of Mre11 endonuclease. We found that *rpn11-E169G* suppressed the DNA damage sensitivity of both wild-type and *sae2*Δ cells carrying the nuclease-defective *mre11-H125N* allele (Figure 2D), indicating that the suppression of *sae2*Δ DNA damage sensitivity does not require Mre11 nuclease activity. Conversely, it was unable to suppress the DNA damage sensitivity of *sae2*Δ cells lacking Mre11 (Figure 2E). These findings indicate that the *rpn11-E169G* allele requires the physical presence of the MRX complex, but not its nuclease activity, to bypass the function of Sae2 in supporting DNA damage resistance. Finally, the *rpn11-E169G* mutation does not bypass the requirement of HR to support DNA damage resistance, as it was unable to suppress the DNA damage sensitivity of *rad52*Δ cells (Figure 2F).

Interestingly, DSB resection occurred more efficiently in *rpn11-E169G* cells compared to wild-type cells (Figures 2B and 2C). To assess whether this increased DSB resection is physiologically relevant, we measured the efficiency of DSB repair by single-strand annealing (SSA), a mechanism that repairs a DSB flanked by direct DNA repeats when resection of the DSB ends reaches the complementary DNA sequences that can then anneal.[58] The *rpn11-E169G* allele was introduced in the YMV45 strain, which carries two tandem repeats of the *LEU2* gene located 4.6 kb apart on chromosome III, with an HO recognition site adjacent to one of the repeats (Figure 3A).[59] This strain also harbors a *GAL-HO* construct to induce HO expression upon galactose addition. Accumulation of the SSA repair products after HO induction occurred more efficiently in *rpn11-E169G* cells compared to wild-type cells (Figures 3B and 3C), indicating that the *rpn11-E169G* mutation improves DSB repair by SSA.

The *rpn11-E169G* allele suppresses the resection defect of *exo1*Δ but not of *exo1*Δ *sgs1*Δ cells

The MRX complex not only provides the nuclease activity to initiate DSB resection but also stimulates long-range resection independently of Mre11 endonuclease by promoting the association of both Exo1 and Sgs1-Dna2 with the DSB ends.[26,27] The finding that the resection products accumulated more efficiently in galactose-induced *rpn11-E169G* cells compared to wild-type cells (Figures 2B and 2C) raises the possibility that the *rpn11-E169G* mutation might enhance the resection activities of Exo1 and/or Sgs1-Dna2. Thus, we investigated whether the *rpn11-E169G* allele could suppress the DNA damage sensitivity of cells lacking Exo1 and Sgs1, or carrying the temperature-sensitive *dna2-1* allele. As *exo1*Δ, *sgs1*Δ, and the *dna2-1* cells are primarily sensitive to CPT, we compared their CPT sensitivity either in the presence or in the absence of *rpn11-E169G*. The *rpn11-E169G* allele restored resistance to CPT of *exo1*Δ (Figure 4A), *sgs1*Δ (Figure 4B), and *dna2-1* (Figure 4C) cells. However, it failed to alleviate the sensitivity to DNA-damaging agents of cells devoid of both Exo1 and Sgs1 (Figure 4D), indicating that the suppression requires the presence of either or both Exo1 and Sgs1-Dna2.

While *sgs1*Δ cells show no resection defect, resection of the HO-induced DSB in *exo1*Δ cells does not extend beyond the *Ssp*I site located 3.5 kb from the HO-cut site.[60] By contrast, the generation of ssDNA in cells lacking both Exo1 and Sgs1 is confined to a region of 100–300 nucleotides from the DSB ends, due to the action of Mre11 nuclease activity.[7,8,14,15] Therefore, to investigate the effect of *rpn11-E169G* on Exo1- and Sgs1-mediated DSB resection, we introduced the *rpn11-E169G* mutation into *exo1*Δ and *exo1*Δ *sgs1*Δ cells. We observed longer resection products in *exo1*Δ *rpn11-E169G* cells compared to *exo1*Δ cells that, as expected, accumulated mainly r1 and r2 resection products (Figures 5A and 5B), indicating that *rpn11-E169G* suppresses the resection defect of *exo1*Δ cells. Conversely and consistent with the failure of *rpn11-E169G* to restore DNA damage resistance of *exo1*Δ *sgs1*Δ cells (Figure 4D), the *rpn11-E169G* mutation did not suppress the resection defect of *exo1*Δ *sgs1*Δ cells (Figure 5C).

Given that the detection of *Ssp*I-resistant ssDNA by Southern blotting only assesses resection events that go beyond the *Ssp*I site located 0.9 kb from the HO-cut site, we also used a quantitative PCR (qPCR)-based approach to monitor the generation of ssDNA close to the DSB end in *exo1*Δ *sgs1*Δ and *exo1*Δ *sgs1*Δ *rpn11-E169G* cells. This method, in addition to utilizing the *Ssp*I sites used in the Southern blot, also relies on two *Rsa*I cut sites situated at distances of 0.15 and 0.65 kb from the HO-induced DSB (Figure 2A). Resection extending beyond these sites leaves the DNA region uncut, allowing its amplification by PCR with primers surrounding the restriction site. We found that ssDNA in both *exo1*Δ *sgs1*Δ and *exo1*Δ *sgs1*Δ *rpn11-E169G* cells can be detected in close proximity to the HO-cut site (0.15 kb) but not at more distant locations (0.65 and 0.9 kb) (Figure 5D). This finding confirms that the *rpn11-E169G* mutation does not suppress the resection defect of *exo1*Δ *sgs1*Δ cells, indicating that the enhanced resection in *rpn11-E169G* cells requires the presence of either Exo1 or Sgs1, or both.

The *rpn11-E169G* mutation increases Exo1 and Dna2 protein levels

Rpn11 is a deubiquitylating enzyme that plays a critical role in protein degradation by removing ubiquitin chains from substrates that are being targeted for degradation. This function is crucial for the proper functioning of the proteasome and efficient proteolysis.[49] As Exo1 overexpression can partially bypass the requirement of Sae2 to support DNA damage resistance,[61] one possible explanation for the suppression of the phenotypes due to the loss of Sae2 or of either Exo1 or Sgs1-Dna2 is that the *rpn11-E169G* allele increases the levels of Exo1, Sgs1, and/or Dna2 proteins. To test this hypothesis, we compared the amount of Exo1, Dna2, and Sgs1 in exponentially growing wild-type and *rpn11-E169G* cells, both before and after the addition of phleomycin. In the absence of DNA damage, the amounts of Exo1 and Dna2 were higher in

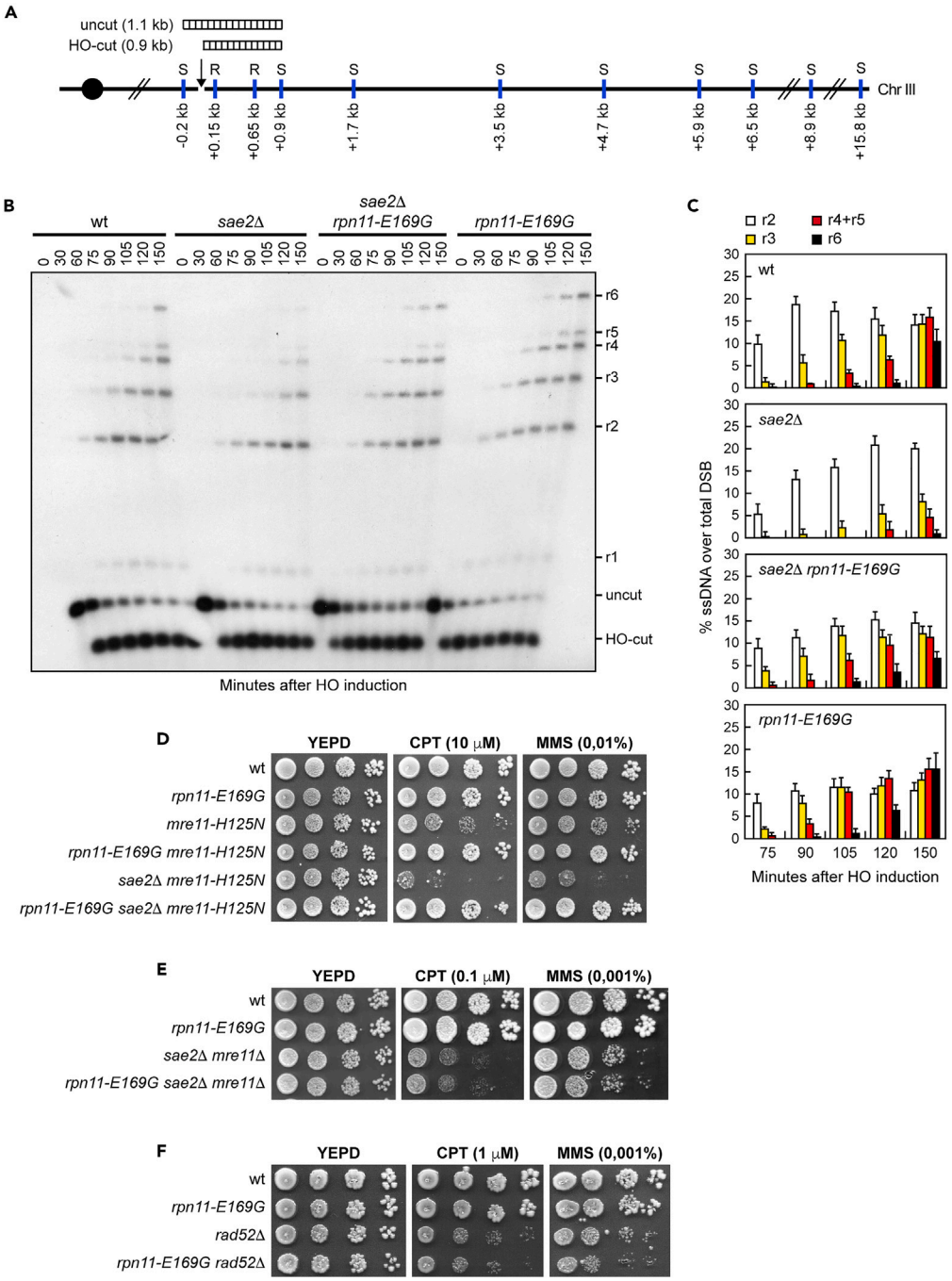

Figure 2. The *rpn11-E169G* mutation suppresses the resection defect of *sae2Δ* cells

(A) Schematic representation of the *MAT* locus and the distance of *Rsa*I (R) and *Ssp*I (S) restriction sites from the HO-cut site. The DNA fragments detected in (B) before (uncut) and after HO cleavage (HO-cut) were also indicated.

(B) DSB resection. Cell cultures exponentially growing in YEPR at 25°C were transferred to YEPRG at 25°C (time zero) to induce HO expression. *Ssp*I-digested genomic DNA prepared at the indicated times after HO induction was separated on alkaline agarose gel and hybridized with a single-stranded *MAT* probe that anneals to the unresected 3′ end at one side of the break. 5′-3′ resection progressively eliminates *Ssp*I sites, producing larger *Ssp*I fragments (r1 through r6) that can be detected by the probe.

(C) Densitometric analysis. The experiment as in (B) was independently repeated three times, and the mean values are represented with error bars denoting SD.

(D–F) Exponentially growing cells were serially diluted (1:10), and each dilution was spotted out onto YEPD plates with or without CPT or MMS that were incubated at 25°C.

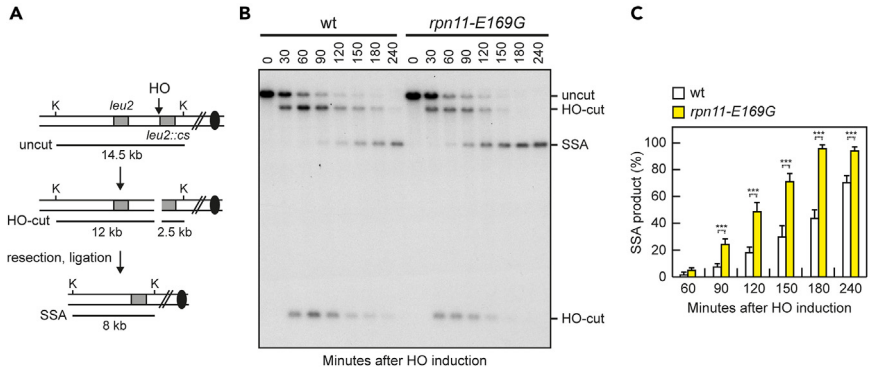

Figure 3. The *rpn11-E169G* mutation increases DSB repair by SSA

(A) Schematic representation of the YMV45 chromosome III region, where a unique HO-cut site is adjacent to the *leu2::cs* sequence, which is 4.6 kb apart from the homologous *leu2* sequence. HO-induced DSB results in generation of 12 kb and 2.5 kb DNA fragments (HO-cut) that can be detected by Southern blot analysis with a *LEU2* probe of *Kpn*I-digested genomic DNA. DSB repair by SSA generates a product of 8 kb (SSA). K, *Kpn*I.

(B) Cell cultures of YMV45 derivative strains exponentially growing in YEPR at 25°C were transferred to YEPRG at 25°C (time zero). Southern blot analysis of *Kpn*I-digested genomic DNA.

(C) Densitometric analysis of the SSA product. The experiment as in (B) was independently repeated three times, and the mean values are represented with error bars denoting SD. ***$p < 0.005$, *t*-test.

rpn11-E169G cells than in wild-type cells (Figures 6A and 6B). The addition of phleomycin did not significantly increase the levels of Exo1 and Dna2 in either cell type (Figures 6A and 6B). However, as previously reported,[62–64] it decreased Dna2 electrophoretic mobility due to phosphorylation events and increased Rad51 expression 6 h after phleomycin addition (Figures 6A and 6B). In contrast, the expression of the *rpn11-E169G* allele did not increase the amount of Sgs1, regardless of whether DNA damage was present or not (Figure 6C). The elevated levels of Exo1 and Dna2 in *rpn11-E169G* cells, both in the absence and in the presence of DNA damage, were not due to higher *EXO1* and *DNA2* RNA levels. In fact, similar amounts of *EXO1* and *DNA2* RNA were detected by quantitative reverse-transcription PCR (RT-qPCR) in both wild-type and *rpn11-E169G* cells regardless of phleomycin exposure (Figure 6D). This finding suggests that Exo1 and Dna2 are normally degraded in a proteasome-dependent manner independently of DNA damage.

The *rpn11-E169G* mutation also leads to an increased association of Exo1 and Dna2 with DNA DSB ends. Chromatin immunoprecipitation (ChIP) coupled with qPCR analysis showed that the levels of Exo1 and Dna2 bound at the HO-induced DSB site were higher in *rpn11-E169G* cells compared to wild-type cells (Figures 6E and 6F), indicating that the recruitment of these proteins at DSBs in a wild-type context has not reached saturation.

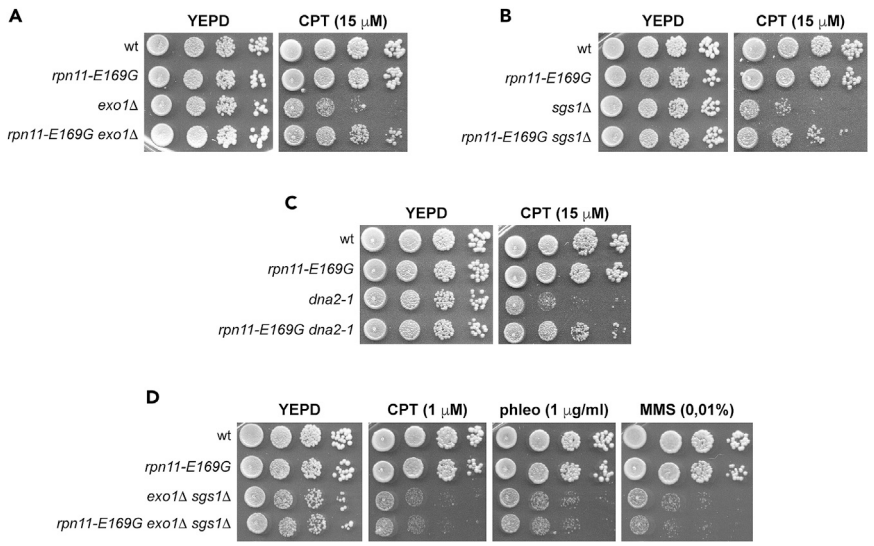

Figure 4. The *rpn11-E169G* mutation suppresses the CPT sensitivity of *exo1Δ* and *sgs1Δ* cells, but not that of *exo1Δ sgs1Δ* cells

(A–D) Exponentially growing cells were serially diluted (1:10), and each dilution was spotted out onto YEPD plates with or without CPT, phleomycin, or MMS that were incubated at 25°C.

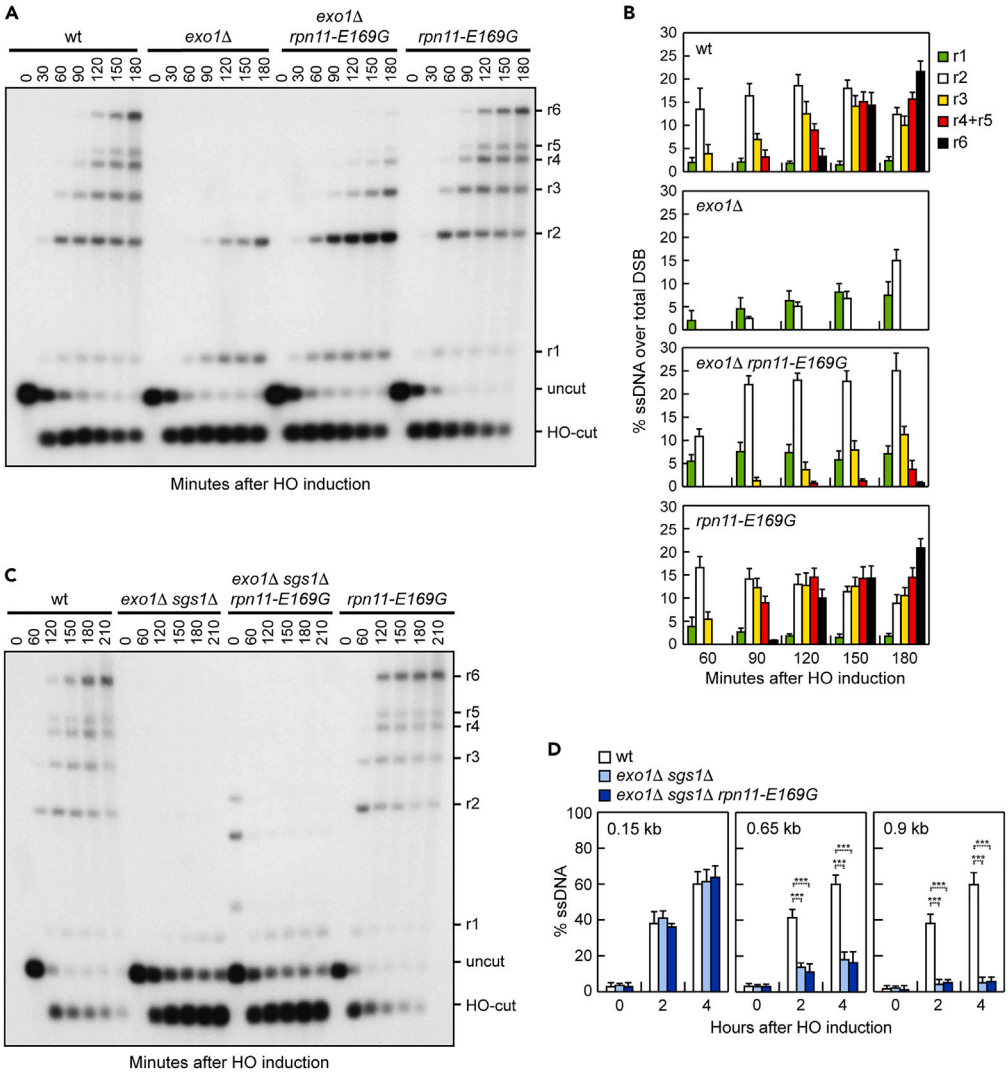

Figure 5. The *rpn11-E169G* mutation suppresses the resection defect of *exo1Δ* but not of *exo1Δ sgs1Δ* cells

(A) Cell cultures of JKM139 derivative strains exponentially growing in YEPR at 25°C were transferred to YEPRG at 25°C (time zero). Southern blot analysis of *Ssp*I-digested genomic DNA after alkaline gel electrophoresis with a probe that anneals to the unresected strand. 5′-3′ resection progressively eliminates *Ssp*I sites (S), producing *Ssp*I fragments (r1 through r6) detected by the probe.

(B) The experiment as in (A) has been independently repeated three times, and the mean values are represented with error bars denoting SD.

(C) Cell cultures of JKM139 derivative strains exponentially growing in YEPR at 25°C were transferred to YEPRG at 25°C (time zero). Southern blot analysis of *Ssp*I-digested genomic DNA was performed as described in (A).

(D) Quantification of ssDNA by qPCR at the indicated distances from the HO-cut site. Plotted values are the mean values of three independent experiments, with error bars denoting SD. ***$p < 0.005$, *t*-test.

Exo1 and Dna2 are ubiquitylated

In *S. cerevisiae*, Dna2 has been shown to undergo degradation in response to caffeine treatment in a manner dependent on the 26S proteasome activity,[42] whereas EXO1 appears to be ubiquitylated and degraded following DNA damage in human cells.[46] Considering that proteins are targeted to the proteasome primarily through the attachment of polyubiquitin chains, we investigated whether Exo1 and Dna2 are ubiquitylated *in vivo*. For this purpose, wild-type and *rpn11-E169G* strains, both expressing Myc-tagged Exo1 and HA-tagged Dna2 from their native chromosomal loci, were transformed with a high-copy-number plasmid containing a construct for the expression of hexa-histidine-tagged ubiquitin (His-Ubi) under a copper-inducible promoter. Following induction with copper sulfate, His-Ubi-protein conjugates were isolated using nickel-nitrilotriacetic acid (Ni-NTA) resin. Western blot analysis was then performed with anti-Myc and anti-HA antibodies to detect Exo1-Myc and Dna2-HA, respectively. We observed slower-migrating forms of Exo1 and Dna2 in samples expressing histidine-tagged-Ubi (Figures 6G and 6H). These bands increased in amount in *rpn11-E169G* cells, whereas these were absent in samples where

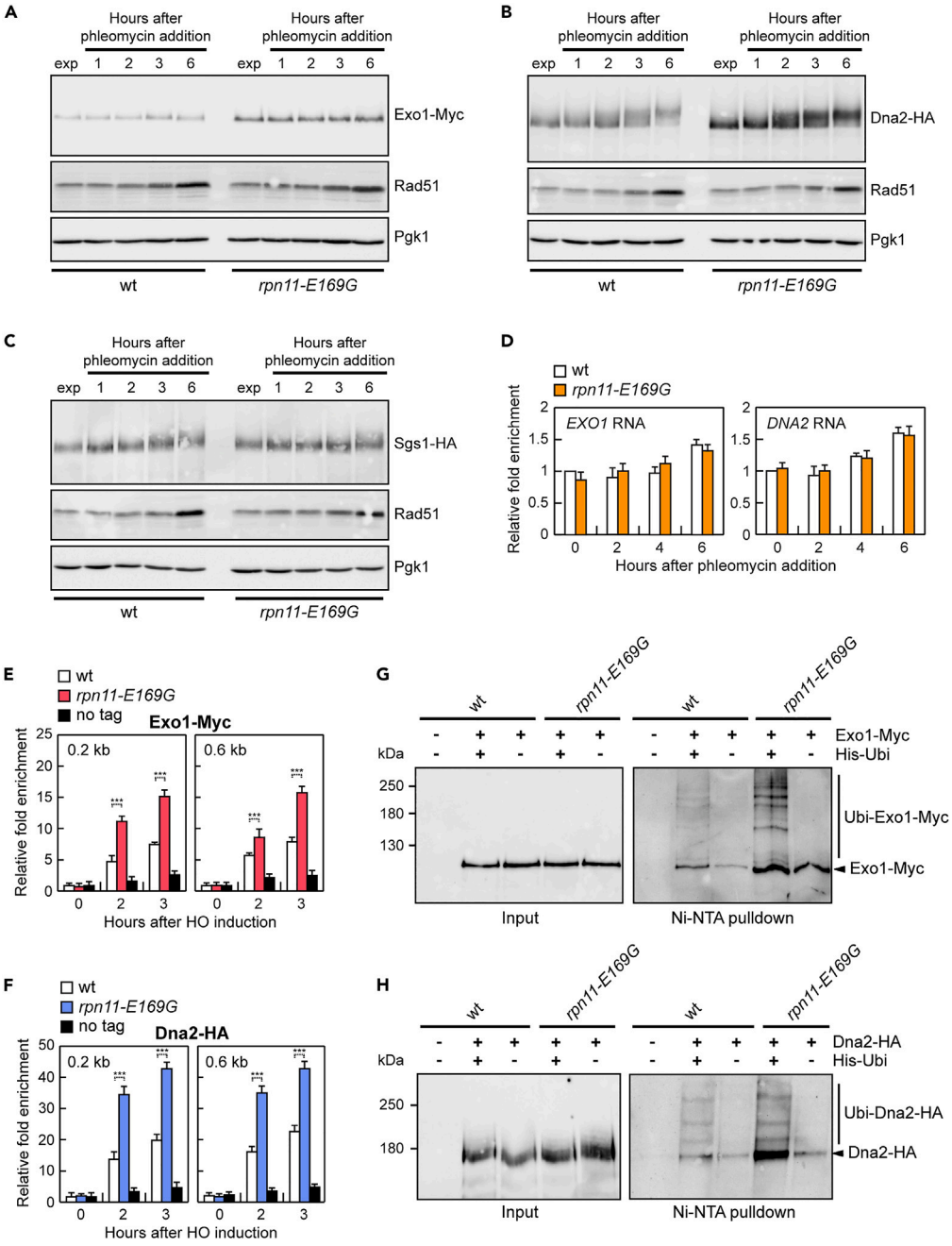

Figure 6. Exo1 and Dna2 protein levels and ubiquitylation

(A–C) Protein extracts were prepared from cells exponentially growing in YEPD at 25°C either untreated (exp) or after addition of 10 μg/mL phleomycin.

(D) Total RNA extracted from cells exponentially growing in YEPD at 25°C (time zero) or at different time points after phleomycin addition (10 μg/mL) was subjected to RT-qPCR with primer pairs located into the *EXO1* and *DNA2* coding sequences. Data are expressed as enrichment of RNA relative to wild type at time zero that was set up at 1. Plotted values are the mean values of three independent experiments, with error bars denoting SD.

(E and F) ChIP and qPCR. Exo1-Myc (E) and Dna2-HA (F) ChIP at the indicated distances from the HO-induced DSB. Data are expressed as fold enrichment at the HO-cut site over that at the non-cleavable *ARO1* locus, after normalization to the corresponding input for each time point. Fold enrichment was normalized to cut efficiency. Plotted values are the mean values ± SD from three independent experiments. ***$p < 0.005$, *t*-test.

(G and H) Ni-NTA affinity pulldowns of 6xHis-Ubi-protein conjugates. Ni-NTA pull-down assays were carried out using cell extracts from wild-type and *rpn11-E169G* strains expressing Exo1-Myc (G) or Dna2-HA (H) at endogenous levels and overexpressing 6xHis-tagged ubiquitin from the *CUP1* promoter. Exo1 and Dna2 ubiquitylation was revealed by western blotting with an anti-Myc (G) and an anti-HA (H) antibody, respectively.

Exo1 and Dna2 were untagged or where histidine-tagged-Ubi was not induced (Figures 6G and 6H), indicating that the slower-migrating variants of Exo1 and Dna2 represent modifications with multiple ubiquitin molecules.

DISCUSSION

The process of DSB resection serves important functions not only in HR but also in DNA damage signaling and in determining the balance between HR and NHEJ repair mechanisms.[1–4] However, unscheduled or extensive resection can pose risks to genomic integrity, as ssDNA created by resection is vulnerable to chemical changes or degradation by nucleases and these events can lead to clustered mutations or loss of single-stranded overhangs.[65,66] Furthermore, an excess of ssDNA can exhaust the RPA nuclear pool, which can lead to replication fork breakage.[67] Finally, the resected ssDNA tracts can become substrates for mutagenic repair mechanisms, such as SSA and microhomology-mediated end joining that can result in deletions.[68] The overcoming of these threats needs a tight control of end resection.

Current models of DSB resection posit that MRX-Sae2 catalyzes resection initiation, and this is followed by long-range resection performed by Exo1 and Dna2-Sgs1, which partially overlap in function as indicated by synergistic defects in resection upon inactivation of both of them.[7,8]

Here, we found that mutations in the proteasome components can bypass the need for Sae2 in DNA damage resistance and DSB resection. In particular, the *rpn11-E169G* mutation affecting the Rpn11 proteasome subunit causes hyper-resection by itself and increases the amount of both Exo1 and Dna2, highlighting a function of the proteasome in restricting DSB resection by targeting Exo1 and Dna2 for degradation. The increased Exo1 and Dna2 protein levels allow to compensate for the lack of Exo1 or Sgs1-Dna2, but not when Exo1 and Sgs1-Dna2 are simultaneously absent. Consistent with the knowledge that proteins are targeted to the proteasome primarily through the attachment of polyubiquitin chains, we showed that both Exo1 and Dna2 are modified with multiple ubiquitin molecules, indicating that proteasome-mediated degradation negatively regulates long-range resection by controlling the levels of Exo1 and Dna2. By contrast, the amount of Sgs1 is not increased in *rpn11-E169G* cells, implying that the Sgs1 protein level is not a limiting factor for the resection activity of the Sgs1-Dna2 complex.

Interestingly, although the identified proteasome mutations suppress the sensitivity of *sae2*Δ cells to CPT and MMS, they only partially restore resistance to phleomycin. Considering that the *rpn11-E169G* mutation fully suppresses the resection defect of *sae2*Δ cells, this finding suggests that end resection is more critical in repairing CPT-induced DNA lesions, which may be transformed to DSBs and/or to unusual replication intermediates requiring HR for repair and resolution. This hypothesis aligns with the finding that deletion of Ku70, which suppresses the *sae2*Δ resection defect by relieving inhibition of Exo1,[26,27] restores resistance to CPT and MMS of *sae2*Δ cells but fails to reduce their phleomycin sensitivity.[69] In contrast, the repair of phleomycin-induced DNA lesions appears to depend on the end tethering of DNA DSBs, as the *ku70-C85Y* mutation, which suppresses the end tethering but not the resection defect of *sae2*Δ cells, partially restores phleomycin resistance.[69]

While human EXO1 turns out to be ubiquitylated and rapidly degraded following DNA damage,[46] in yeast the proteasome-mediated control of Exo1 and Dna2 protein levels is not induced by DNA damage, implying a constitutive negative regulation of Exo1 and Dna2 also under normal conditions. Indeed, Dna2 is involved in Okazaki fragment maturation,[70] and Exo1 and Sgs1-Dna2 have been implicated in the processing of replication intermediates to allow repair/restart of stalled replication forks and/or to prevent accumulation of replication-associated DSBs.[71] Although controlled degradation of replication forks by nucleases can be a relevant mechanism to recover replication fork blockage, unrestricted Exo1 and Dna2 nuclease activity could destroy the fork structure and prevent the restart of DNA synthesis, leading to genome instability.

In conclusion, our study uncovers a role for the proteasome in regulating the DNA damage response by mediating the degradation of the key resection nucleases Exo1 and Dna2. This regulation is part of a broader control network over these nucleases, including protein-protein interactions,[26,27,72–74] post-translational modifications,[22,43–45,75–77] and the regulation of mRNA biogenesis.[78] The existence of such multiple layers of regulation underscores the need for tight control over Exo1 and Dna2 activities to avoid excessive DNA resection that could lead to genomic instability. Increased levels of human DNA2 and EXO1 have been observed in a variety of tumors, where they are thought to counteract replication stress.[79,80] Since elevated replication stress is a common feature of cancer cells, overexpression of EXO1 and DNA2 may play a role in helping cancer cells to overcome this barrier. Thus, our findings identify a mechanism that helps to restrict Exo1 and Dna2 functions to ensure genome stability.

Limitations of the study

Our work sheds light on the role of the proteasome in restraining DSB resection by negatively controlling the abundance of the long-range resection nucleases. However, the E3 ubiquitin ligase(s) involved in Exo1 and Dna2 ubiquitylation remains undefined. Furthermore, the pathological outcomes resulting from unscheduled DNA degradation upon proteasome dysfunction at DNA DSBs and stalled replication forks remain to be determined and will need further experimental investigation to be addressed.

STAR★METHODS

Detailed methods are provided in the online version of this paper and include the following:

- KEY RESOURCES TABLE
- RESOURCE AVAILABILITY
  - Lead contact

SUPPLEMENTAL INFORMATION

Supplemental information can be found online at https://doi.org/10.1016/j.isci.2024.110373.

ACKNOWLEDGMENTS

We thank J. Haber for providing yeast strains. We are also grateful to R. Fraschini for providing plasmids and for assistance with the detection of ubiquitin conjugates and M. Clerici for critical reading of the manuscript. This work was supported by Fondazione AIRC under IG 2022 - ID. 27001 project to M.P.L. and Progetti di Ricerca di Interesse Nazionale (PRIN) 2020 and PRIN 2022 to M.P.L.

AUTHOR CONTRIBUTIONS

Conceptualization, M.G. and M.P.L.; investigation, M.G., C.R., E.C., P.P., and D.B.; writing – original draft, M.P.L.; writing – review and editing, M.G., C.R., E.C., P.P., D.B., and M.P.L.; supervision, M.P.L.; funding acquisition, M.P.L.

DECLARATION OF INTERESTS

The authors declare no competing interests.

Received: February 22, 2024
Revised: April 30, 2024
Accepted: June 21, 2024
Published: June 22, 2024

REFERENCES

1. Stinson, B.M., and Loparo, J.J. (2021). Repair of DNA double-strand breaks by the nonhomologous end joining pathway. Annu. Rev. Biochem. *90*, 137–164. https://doi.org/10.1146/annurev-biochem-080320-110356.
2. Mehta, A., and Haber, J.E. (2014). Sources of DNA double-strand breaks and models of recombinational DNA repair. Cold Spring Harb. Perspect. Biol. *6*, a016428. https://doi.org/10.1101/cshperspect.a016428.
3. Cejka, P., and Symington, L.S. (2021). DNA end resection: mechanism and control. Annu. Rev. Genet. *55*, 285–307. https://doi.org/10.1146/annurev-genet-071719-020312.
4. Pizzul, P., Casari, E., Gnugnoli, M., Rinaldi, C., Corallo, F., and Longhese, M.P. (2022). The DNA damage checkpoint: A tale from budding yeast. Front. Genet. *13*, 995163. https://doi.org/10.3389/fgene.2022.995163.
5. Mantiero, D., Clerici, M., Lucchini, G., and Longhese, M.P. (2007). Dual role for *Saccharomyces cerevisiae* Tel1 in the checkpoint response to double-strand breaks. EMBO Rep. *8*, 380–387. https://doi.org/10.1038/sj.embor.7400911.
6. Cannavo, E., and Cejka, P. (2014). Sae2 promotes dsDNA endonuclease activity within Mre11-Rad50-Xrs2 to resect DNA breaks. Nature *514*, 122–125. https://doi.org/10.1038/nature13771.
7. Mimitou, E.P., and Symington, L.S. (2008). Sae2, Exo1 and Sgs1 collaborate in DNA double-strand break processing. Nature *455*, 770–774. https://doi.org/10.1038/nature07312.
8. Zhu, Z., Chung, W.H., Shim, E.Y., Lee, S.E., and Ira, G. (2008). Sgs1 helicase and two nucleases Dna2 and Exo1 resect DNA double-strand break ends. Cell *134*, 981–994. https://doi.org/10.1016/j.cell.2008.08.037.
9. Cejka, P., Cannavo, E., Polaczek, P., Masuda-Sasa, T., Pokharel, S., Campbell, J.L., and Kowalczykowski, S.C. (2010). DNA end resection by Dna2-Sgs1-RPA and its stimulation by Top3-Rmi1 and Mre11-Rad50-Xrs2. Nature *467*, 112–116. https://doi.org/10.1038/nature09355.
10. Niu, H., Chung, W.H., Zhu, Z., Kwon, Y., Zhao, W., Chi, P., Prakash, R., Seong, C., Liu, D., Lu, L., et al. (2010). Mechanism of the ATP-dependent DNA end-resection machinery from *Saccharomyces cerevisiae*. Nature *467*, 108–111. https://doi.org/10.1038/nature09318.
11. Garcia, V., Phelps, S.E.L., Gray, S., and Neale, M.J. (2011). Bidirectional resection of DNA double-strand breaks by Mre11 and Exo1. Nature *479*, 241–244. https://doi.org/10.1038/nature10515.
12. Nimonkar, A.V., Genschel, J., Kinoshita, E., Polaczek, P., Campbell, J.L., Wyman, C., Modrich, P., and Kowalczykowski, S.C. (2011). BLM-DNA2-RPA-MRN and EXO1-BLM-RPA-MRN constitute two DNA end resection machineries for human DNA break repair. Genes Dev. *25*, 350–362. https://doi.org/10.1101/gad.2003811.
13. Shibata, A., Moiani, D., Arvai, A.S., Perry, J., Harding, S.M., Genois, M.M., Maity, R., van Rossum-Fikkert, S., Kertokalio, A., Romoli, F., et al. (2014). DNA double-strand break repair pathway choice is directed by distinct MRE11 nuclease activities. Mol. Cell *53*, 7–18. https://doi.org/10.1016/j.molcel.2013.11.003.
14. Gobbini, E., Casari, E., Colombo, C.V., Bonetti, D., and Longhese, M.P. (2020). The 9-1-1 complex controls Mre11 nuclease and checkpoint activation during short-range resection of DNA double-strand breaks. Cell Rep. *33*, 108287. https://doi.org/10.1016/j.celrep.2020.108287.
15. Guo, X., Hum, Y.F., Lehner, K., and Jinks-Robertson, S. (2017). Regulation of hetDNA length during mitotic double-strand break repair in yeast. Mol. Cell *67*, 539–549.e4. https://doi.org/10.1016/j.molcel.2017.07.009.
16. Kimble, M.T., Johnson, M.J., Nester, M.R., and Symington, L.S. (2023). Long-range DNA

end resection supports homologous recombination by checkpoint activation rather than extensive homology generation. Elife *12*, e84322. https://doi.org/10.7554/eLife.84322.

17. Bonetti, D., Villa, M., Gobbini, E., Cassani, C., Tedeschi, G., and Longhese, M.P. (2015). Escape of Sgs1 from Rad9 inhibition reduces the requirement for Sae2 and functional MRX in DNA end resection. EMBO Rep. *16*, 351–361. https://doi.org/10.15252/embr.201439764.
18. Gobbini, E., Villa, M., Gnugnoli, M., Menin, L., Clerici, M., and Longhese, M.P. (2015). Sae2 function at DNA double-strand breaks is bypassed by dampening Tel1 or Rad53 activity. PLoS Genet. *11*, e1005685. https://doi.org/10.1371/journal.pgen.1005685.
19. Ferrari, M., Dibitetto, D., De Gregorio, G., Eapen, V.V., Rawal, C.C., Lazzaro, F., Tsabar, M., Marini, F., Haber, J.E., and Pellicioli, A. (2015). Functional interplay between the 53BP1-ortholog Rad9 and the Mre11 complex regulates resection, end-tethering and repair of a double-strand break. PLoS Genet. *11*, e1004928. https://doi.org/10.1371/journal.pgen.1004928.
20. Lydall, D., and Weinert, T. (1995). Yeast checkpoint genes in DNA damage processing: implications for repair and arrest. Science *270*, 1488–1491. https://doi.org/10.1126/science.270.5241.1488.
21. Yu, T.Y., Kimble, M.T., and Symington, L.S. (2018). Sae2 antagonizes Rad9 accumulation at DNA double-strand breaks to attenuate checkpoint signaling and facilitate end resection. Proc. Natl. Acad. Sci. USA *115*, E11961. https://doi.org/10.1073/pnas.1816539115.
22. Morin, I., Ngo, H.P., Greenall, A., Zubko, M.K., Morrice, N., and Lydall, D. (2008). Checkpoint-dependent phosphorylation of Exo1 modulates the DNA damage response. EMBO J. *27*, 2400–2410. https://doi.org/10.1038/emboj.2008.171.
23. Tomita, K., Matsuura, A., Caspari, T., Carr, A.M., Akamatsu, Y., Iwasaki, H., Mizuno, K.i., Ohta, K., Uritani, M., Ushimaru, T., et al. (2003). Competition between the Rad50 complex and the Ku heterodimer reveals a role for Exo1 in processing double-strand breaks but not telomeres. Mol. Cell Biol. *23*, 5186–5197. https://doi.org/10.1128/MCB.23.15.5186-5197.2003.
24. Clerici, M., Mantiero, D., Guerini, I., Lucchini, G., and Longhese, M.P. (2008). The Yku70-Yku80 complex contributes to regulate double-strand break processing and checkpoint activation during the cell cycle. EMBO Rep. *9*, 810–818. https://doi.org/10.1038/embor.2008.121.
25. Zierhut, C., and Diffley, J.F.X. (2008). Break dosage, cell cycle stage and DNA replication influence DNA double strand break response. EMBO J. *27*, 1875–1885. https://doi.org/10.1038/emboj.2008.111.
26. Mimitou, E.P., and Symington, L.S. (2010). Ku prevents Exo1 and Sgs1-dependent resection of DNA ends in the absence of a functional MRX complex or Sae2. EMBO J. *29*, 3358–3369. https://doi.org/10.1038/emboj.2010.193.
27. Shim, E.Y., Chung, W.H., Nicolette, M.L., Zhang, Y., Davis, M., Zhu, Z., Paull, T.T., Ira, G., and Lee, S.E. (2010). *Saccharomyces cerevisiae* Mre11/Rad50/Xrs2 and Ku proteins regulate association of Exo1 and Dna2 with DNA breaks. EMBO J. *29*, 3370–3380. https://doi.org/10.1038/emboj.2010.219.
28. Ngo, G.H.P., and Lydall, D. (2015). The 9-1-1 checkpoint clamp coordinates resection at DNA double strand breaks. Nucleic Acids Res. *43*, 5017–5032. https://doi.org/10.1093/nar/gkv409.
29. Marsella, A., Gobbini, E., Cassani, C., Tisi, R., Cannavo, E., Reginato, G., Cejka, P., and Longhese, M.P. (2021). Sae2 and Rif2 regulate MRX endonuclease activity at DNA double-strand breaks in opposite manners. Cell Rep. *34*, 108906. https://doi.org/10.1016/j.celrep.2021.108906.
30. Khayat, F., Cannavo, E., Alshmery, M., Foster, W.R., Chahwan, C., Maddalena, M., Smith, C., Oliver, A.W., Watson, A.T., Carr, A.M., et al. (2021). Inhibition of MRN activity by a telomere protein motif. Nat. Commun. *12*, 3856. https://doi.org/10.1038/s41467-021-24047-2.
31. Clerici, M., Mantiero, D., Lucchini, G., and Longhese, M.P. (2005). The *Saccharomyces cerevisiae* Sae2 protein promotes resection and bridging of double strand break ends. J. Biol. Chem. *280*, 38631–38638. https://doi.org/10.1074/jbc.M508339200.
32. Usui, T., Ogawa, H., and Petrini, J.H. (2001). A DNA damage response pathway controlled by Tel1 and the Mre11 complex. Mol. Cell *7*, 1255–1266. https://doi.org/10.1016/s1097-2765(01)00270-2.
33. Clerici, M., Mantiero, D., Lucchini, G., and Longhese, M.P. (2006). The *Saccharomyces cerevisiae* Sae2 protein negatively regulates DNA damage checkpoint signalling. EMBO Rep. *7*, 212–218. https://doi.org/10.1038/sj.embor.7400593.
34. Chen, H., Donnianni, R.A., Handa, N., Deng, S.K., Oh, J., Timashev, L.A., Kowalczykowski, S.C., and Symington, L.S. (2015). Sae2 promotes DNA damage resistance by removing the Mre11-Rad50-Xrs2 complex from DNA and attenuating Rad53 signaling. Proc. Natl. Acad. Sci. USA *112*, E1880–E1887. https://doi.org/10.1073/pnas.1503331112.
35. Puddu, F., Oelschlaegel, T., Guerini, I., Geisler, N.J., Niu, H., Herzog, M., Salguero, I., Ochoa-Montaño, B., Viré, E., Sung, P., et al. (2015). Synthetic viability genomic screening defines Sae2 function in DNA repair. EMBO J. *34*, 1509–1522. https://doi.org/10.15252/embj.201590973.
36. Finley, D. (2009). Recognition and processing of ubiquitin-protein conjugates by the proteasome. Annu. Rev. Biochem. *78*, 477–513. https://doi.org/10.1146/annurev.biochem.78.081507.101607.
37. Challa, K., Schmid, C.D., Kitagawa, S., Cheblal, A., Iesmantavicius, V., Seeber, A., Amitai, A., Seebacher, J., Hauer, M.H., Shimada, K., and Gasser, S.M. (2021). Damage-induced chromatome dynamics link ubiquitin ligase and proteasome recruitment to histone loss and efficient DNA repair. Mol. Cell *81*, 811–829.e6. https://doi.org/10.1016/j.molcel.2020.12.021.
38. Krogan, N.J., Lam, M.H.Y., Fillingham, J., Keogh, M.C., Gebbia, M., Li, J., Datta, N., Cagney, G., Buratowski, S., Emili, A., and Greenblatt, J.F. (2004). Proteasome involvement in the repair of DNA double-strand breaks. Mol. Cell *16*, 1027–1034. https://doi.org/10.1016/j.molcel.2004.11.033.
39. Ustrell, V., Hoffman, L., Pratt, G., and Rechsteiner, M. (2002). PA200, a nuclear proteasome activator involved in DNA repair. EMBO J. *21*, 3516–3525. https://doi.org/10.1093/emboj/cdf333.
40. Blickwedehl, J., McEvoy, S., Wong, I., Kousis, P., Clements, J., Elliott, R., Cresswell, P., Liang, P., and Bangia, N. (2007). Proteasomes and proteasome activator 200 kDa (PA200) accumulate on chromatin in response to ionizing radiation. Radiat. Res. *167*, 663–674. https://doi.org/10.1667/RR0690.1.
41. Levy-Barda, A., Lerenthal, Y., Davis, A.J., Chung, Y.M., Essers, J., Shao, Z., van Vliet, N., Chen, D.J., Hu, M.C.T., Kanaar, R., et al. (2011). Involvement of the nuclear proteasome activator PA28γ in the cellular response to DNA double-strand breaks. Cell Cycle *10*, 4300–4310. https://doi.org/10.4161/cc.10.24.18642.
42. Tsabar, M., Eapen, V.V., Mason, J.M., Memisoglu, G., Waterman, D.P., Long, M.J., Bishop, D.K., and Haber, J.E. (2015). Caffeine impairs resection during DNA break repair by reducing the levels of nucleases Sae2 and Dna2. Nucleic Acids Res. *43*, 6889–6901. https://doi.org/10.1093/nar/gkv520.
43. Ranjha, L., Levikova, M., Altmannova, V., Krejci, L., and Cejka, P. (2019). Sumoylation regulates the stability and nuclease activity of *Saccharomyces cerevisiae* Dna2. Commun. Biol. *2*, 174. https://doi.org/10.1038/s42003-019-0428-0.
44. El-Shemerly, M., Hess, D., Pyakurel, A.K., Moselhy, S., and Ferrari, S. (2008). ATR-dependent pathways control hEXO1 stability in response to stalled forks. Nucleic Acids Res. *36*, 511–519. https://doi.org/10.1093/nar/gkm1052.
45. Bologna, S., Altmannova, V., Valtorta, E., Koenig, C., Liberali, P., Gentili, C., Anrather, D., Ammerer, G., Pelkmans, L., Krejci, L., and Ferrari, S. (2015). Sumoylation regulates EXO1 stability and processing of DNA damage. Cell Cycle *14*, 2439–2450. https://doi.org/10.1080/15384101.2015.1060381.
46. Tomimatsu, N., Mukherjee, B., Harris, J.L., Boffo, F.L., Hardebeck, M.C., Potts, P.R., Khanna, K.K., and Burma, S. (2017). DNA-damage-induced degradation of EXO1 exonuclease limits DNA end resection to ensure accurate DNA repair. J. Biol. Chem. *292*, 10779–10790. https://doi.org/10.1074/jbc.M116.772475.
47. Xie, Y., Liu, Y.K., Guo, Z.P., Guan, H., Liu, X.D., Xie, D.F., Jiang, Y.G., Ma, T., and Zhou, P.K. (2020). RBX1 prompts degradation of EXO1 to limit the homologous recombination pathway of DNA double-strand break repair in G1 phase. Cell Death Differ. *27*, 1383–1397. https://doi.org/10.1038/s41418-019-0424-4.
48. Deng, C., Brown, J.A., You, D., and Brown, J.M. (2005). Multiple endonucleases function to repair covalent topoisomerase I complexes in *Saccharomyces cerevisiae*. Genetics *170*, 591–600. https://doi.org/10.1534/genetics.104.028795.
49. Finley, D., Ulrich, H.D., Sommer, T., and Kaiser, P. (2012). The ubiquitin-proteasome system of *Saccharomyces cerevisiae*. Genetics *192*, 319–360. https://doi.org/10.1534/genetics.112.140467.
50. Bard, J.A.M., Goodall, E.A., Greene, E.R., Jonsson, E., Dong, K.C., and Martin, A. (2018). Structure and function of the 26S proteasome. Annu. Rev. Biochem. *87*, 697–724. https://doi.org/10.1146/annurev-biochem-062917-011931.
51. Yao, T., and Cohen, R.E. (2002). A cryptic protease couples deubiquitination and degradation by the proteasome. Nature *419*, 403–407. https://doi.org/10.1038/nature01071.

52. Verma, R., Aravind, L., Oania, R., McDonald, W.H., Yates, J.R., 3rd, Koonin, E.V., and Deshaies, R.J. (2002). Role of Rpn11 metalloprotease in deubiquitination and degradation by the 26S proteasome. Science *298*, 611–615. https://doi.org/10.1126/science.1075898.
53. Maytal-Kivity, V., Reis, N., Hofmann, K., and Glickman, M.H. (2002). MPN+, a putative catalytic motif found in a subset of MPN domain proteins from eukaryotes and prokaryotes, is critical for Rpn11 function. BMC Biochem. *3*, 28. https://doi.org/10.1186/1471-2091-3-28.
54. Butler, L.R., Densham, R.M., Jia, J., Garvin, A.J., Stone, H.R., Shah, V., Weekes, D., Festy, F., Beesley, J., and Morris, J.R. (2012). The proteasomal de-ubiquitinating enzyme POH1 promotes the double-strand DNA break response. EMBO J. *31*, 3918–3934. https://doi.org/10.1038/emboj.2012.232.
55. Kakarougkas, A., Ismail, A., Katsuki, Y., Freire, R., Shibata, A., and Jeggo, P.A. (2013). Co-operation of BRCA1 and POH1 relieves the barriers posed by 53BP1 and RAP80 to resection. Nucleic Acids Res. *41*, 10298–10311. https://doi.org/10.1093/nar/gkt802.
56. Lee, S.E., Moore, J.K., Holmes, A., Umezu, K., Kolodner, R.D., and Haber, J.E. (1998). *Saccharomyces* Ku70, mre11/rad50 and RPA proteins regulate adaptation to G2/M arrest after DNA damage. Cell *94*, 399–409. https://doi.org/10.1016/s0092-8674(00)81482-8.
57. White, C.I., and Haber, J.E. (1990). Intermediates of recombination during mating type switching in *Saccharomyces cerevisiae*. EMBO J. *9*, 663–673. https://doi.org/10.1002/j.1460-2075.1990.tb08158.x.
58. Ivanov, E.L., Sugawara, N., Fishman-Lobell, J., and Haber, J.E. (1996). Genetic requirements for the single-strand annealing pathway of double-strand break repair in *Saccharomyces cerevisiae*. Genetics *142*, 693–704. https://doi.org/10.1093/genetics/142.3.693.
59. Vaze, M.B., Pellicioli, A., Lee, S.E., Ira, G., Liberi, G., Arbel-Eden, A., Foiani, M., and Haber, J.E. (2002). Recovery from checkpoint-mediated arrest after repair of a double-strand break requires Srs2 helicase. Mol. Cell *10*, 373–385. https://doi.org/10.1016/s1097-2765(02)00593-2.
60. Gobbini, E., Cassani, C., Vertemara, J., Wang, W., Mambretti, F., Casari, E., Sung, P., Tisi, R., Zampella, G., and Longhese, M.P. (2018). The MRX complex regulates Exo1 resection activity by altering DNA end structure. EMBO J. *37*, e98588. https://doi.org/10.15252/embj.201798588.
61. Menin, L., Ursich, S., Trovesi, C., Zellweger, R., Lopes, M., Longhese, M.P., and Clerici, M. (2018). Tel1/ATM prevents degradation of replication forks that reverse after topoisomerase poisoning. EMBO Rep. *19*, e45535. https://doi.org/10.15252/embr.201745535.
62. Chen, X., Niu, H., Chung, W.H., Zhu, Z., Papusha, A., Shim, E.Y., Lee, S.E., Sung, P., and Ira, G. (2011). Cell cycle regulation of DNA double-strand break end resection by Cdk1-dependent Dna2 phosphorylation. Nat. Struct. Mol. Biol. *18*, 1015–1019. https://doi.org/10.1038/nsmb.2105.
63. Basile, G., Aker, M., and Mortimer, R.K. (1992). Nucleotide sequence and transcriptional regulation of the yeast recombinational repair gene *RAD51*. Mol. Cell Biol. *12*, 3235–3246. https://doi.org/10.1128/mcb.12.7.3235-3246.1992.
64. Shinohara, A., Ogawa, H., and Ogawa, T. (1992). Rad51 protein involved in repair and recombination in S. cerevisiae is a RecA-like protein. Cell *69*, 457–470. https://doi.org/10.1016/0092-8674(92)90447-k.
65. Chen, H., Lisby, M., and Symington, L.S. (2013). RPA coordinates DNA end resection and prevents formation of DNA hairpins. Mol. Cell *50*, 589–600. https://doi.org/10.1016/j.molcel.2013.04.032.
66. Saini, N., and Gordenin, D.A. (2020). Hypermutation in single-stranded DNA. DNA Repair *91*, 102868. https://doi.org/10.1016/j.dnarep.2020.102868.
67. Toledo, L.I., Altmeyer, M., Rask, M.B., Lukas, C., Larsen, D.H., Povlsen, L.K., Bekker-Jensen, S., Mailand, N., Bartek, J., and Lukas, J. (2013). ATR prohibits replication catastrophe by preventing global exhaustion of RPA. Cell *155*, 1088–1103. https://doi.org/10.1016/j.cell.2013.10.043.
68. Al-Zain, A.M., and Symington, L.S. (2021). The dark side of homology-directed repair. DNA Repair *106*, 103181. https://doi.org/10.1016/j.dnarep.2021.103181.
69. Rinaldi, C., Pizzul, P., Casari, E., Mangiagalli, M., Tisi, R., and Longhese, M.P. (2023). The Ku complex promotes DNA end-bridging and this function is antagonized by Tel1/ATM kinase. Nucleic Acids Res. *51*, 1783–1802. https://doi.org/10.1093/nar/gkad062.
70. Levikova, M., and Cejka, P. (2015). The *Saccharomyces cerevisiae* Dna2 can function as a sole nuclease in the processing of Okazaki fragments in DNA replication. Nucleic Acids Res. *43*, 7888–7897. https://doi.org/10.1093/nar/gkv710.
71. Pasero, P., and Vindigni, A. (2017). Nucleases acting at stalled forks: how to reboot the replication program with a few shortcuts. Annu. Rev. Genet. *51*, 477–499. https://doi.org/10.1146/annurev-genet-120116-024745.
72. Karanja, K.K., Lee, E.H., Hendrickson, E.A., and Campbell, J.L. (2014). Preventing over-resection by DNA2 helicase/nuclease suppresses repair defects in Fanconi anemia cells. Cell Cycle *13*, 1540–1550. https://doi.org/10.4161/cc.28476.
73. Zhang, J.M., Liu, X.M., Ding, Y.H., Xiong, L.Y., Ren, J.Y., Zhou, Z.X., Wang, H.T., Zhang, M.J., Yu, Y., Dong, M.Q., and Du, L.L. (2014). Fission yeast Pxd1 promotes proper DNA repair by activating Rad16^{XPF} and inhibiting Dna2. PLoS Biol. *12*, e1001946. https://doi.org/10.1371/journal.pbio.1001946.
74. Chen, X., Kim, I.K., Honaker, Y., Paudyal, S.C., Koh, W.K., Sparks, M., Li, S., Piwnica-Worms, H., Ellenberger, T., and You, Z. (2015). 14-3-3 proteins restrain the Exo1 nuclease to prevent overresection. J. Biol. Chem. *290*, 12300–12312. https://doi.org/10.1074/jbc.M115.644005.
75. Tomimatsu, N., Mukherjee, B., Catherine Hardebeck, M., Ilcheva, M., Vanessa Camacho, C., Louise Harris, J., Porteus, M., Llorente, B., Khanna, K.K., and Burma, S. (2014). Phosphorylation of EXO1 by CDKs 1 and 2 regulates DNA end resection and repair pathway choice. Nat. Commun. *5*, 3561. https://doi.org/10.1038/ncomms4561.
76. Elia, A.E.H., Boardman, A.P., Wang, D.C., Huttlin, E.L., Everley, R.A., Dephoure, N., Zhou, C., Koren, I., Gygi, S.P., and Elledge, S.J. (2015). Quantitative Proteomic Atlas of ubiquitination and acetylation in the DNA damage response. Mol. Cell *59*, 867–881. https://doi.org/10.1016/j.molcel.2015.05.006.
77. Morafraile, E.C., Bugallo, A., Carreira, R., Fernández, M., Martín-Castellanos, C., Blanco, M.G., and Segurado, M. (2020). Exo1 phosphorylation inhibits exonuclease activity and prevents fork collapse in rad53 mutants independently of the 14-3-3 proteins. Nucleic Acids Res. *48*, 3053–3070. https://doi.org/10.1093/nar/gkaa054.
78. Colombo, C.V., Trovesi, C., Menin, L., Longhese, M.P., and Clerici, M. (2017). The RNA binding protein Npl3 promotes resection of DNA double-strand breaks by regulating the levels of Exo1. Nucleic Acids Res. *45*, 6530–6545. https://doi.org/10.1093/nar/gkx347.
79. Kumar, S., Peng, X., Daley, J., Yang, L., Shen, J., Nguyen, N., Bae, G., Niu, H., Peng, Y., Hsieh, H.J., et al. (2017). Inhibition of DNA2 nuclease as a therapeutic strategy targeting replication stress in cancer cells. Oncogenesis *6*, e319. https://doi.org/10.1038/oncsis.2017.15.
80. Peng, G., Dai, H., Zhang, W., Hsieh, H.J., Pan, M.R., Park, Y.Y., Tsai, R.Y.L., Bedrosian, I., Lee, J.S., Ira, G., and Lin, S.Y. (2012). Human nuclease/helicase DNA2 alleviates replication stress by promoting DNA end resection. Cancer Res. *72*, 2802–2813. https://doi.org/10.1158/0008-5472.CAN-11-3152.
81. Raspelli, E., Cassani, C., Lucchini, G., and Fraschini, R. (2011). Budding yeast Dma1 and Dma2 participate in regulation of Swe1 levels and localization. Mol. Biol. Cell *22*, 2185–2197. https://doi.org/10.1091/mbc.E11-02-0127.
82. Casari, E., Gobbini, E., Clerici, M., and Longhese, M.P. (2021). Resection of a DNA double-strand break by alkaline gel electrophoresis and southern blotting. Methods Mol. Biol. *2153*, 33–45. https://doi.org/10.1007/978-1-0716-0644-5_3.
83. Gnugnoli, M., Casari, E., and Longhese, M.P. (2021). The chromatin remodeler Chd1 supports MRX and Exo1 functions in resection of DNA double-strand breaks. PLoS Genet. *17*, e1009807. https://doi.org/10.1371/journal.pgen.1009807.
84. Casari, E., Gobbini, E., Gnugnoli, M., Mangiagalli, M., Clerici, M., and Longhese, M.P. (2021). Dpb4 promotes resection of DNA double-strand breaks and checkpoint activation by acting in two different protein complexes. Nat. Commun. *12*, 4750. https://doi.org/10.1038/s41467-021-25090-9.

STAR★METHODS

KEY RESOURCES TABLE

REAGENT or RESOURCE	SOURCE	IDENTIFIER
Antibodies		
Anti-Rad51	Abcam	Cat#Ab63798; RRID: AB_1142429
Anti-Pgk1	Autoproduction	N/A
Anti-HA (12CA5)	Autoproduction	N/A
Anti-Myc (9E10)	Abcam	Cat#Ab32; RRID: AB_303599
Bacterial and virus strains		
Subcloning Efficiency™ DH5alpha Competent Cells	Invitrogen	Cat#18265017
Chemicals, peptides, and recombinant proteins		
SspI-HF	NEB	Cat#R3132L
RsaI	NEB	Cat#R0167L
KpnI-HF	NEB	Cat#R3142S
Hygromycin B	Roche	Cat#10843555001
G-418 disulfate	Merck	Cat#A1720
Methyl methanesulfonate	Merck	Cat#129925-25G
Phleomycin	Merck	Cat#P9564-100MG
(S)-(+)-Camptothecin	Merck	Cat#C9911-1G
Zymolyase 20T	Nacalai Tesque	Cat#07663-91
Zymolyase 100T	Nacalai Tesque	Cat#0766555
EASYTIDES UTP [alpha-32P]	Revvity	Cat#NEG507T250UC
EASYTIDES ATP [alpha-32P]	Revvity	Cat#NEG512H250UC
Dynabeads Protein G	Invitrogen	Cat#10004D
D(+)-Raffinose pentahydrate	Merck	Cat#83400-100G
D(+)-Galactose	Merck	Cat#48260-500G-F
D(+)-Glucose monohydrate	Merck	Cat#49159-5KG
Yeast Extract Difco	BD	Cat#212750
Peptone DIFCO	BD	Cat#211677
Peptone Oxoid	OXOID	Cat#LP0037T
Yeast extract Oxoid	OXOID	Cat#LP0021T
Agar Bacto Difco	BD	Cat#214030
Agarose LE	EuroClone	Cat#EMR920500
TAE buffer (50X)	EuroClone	Cat#APA16911000
Methanol	Merck	Cat#179337-2.5L
Trichloroacetic acid	Merck	Cat#91230-1KG
RNase A	Roche	Cat#10109169001
Bromophenol Blue sodium salt	Merck	Cat#B6131-25G
Phenylmethanesulfonyl fluoride	Merck	Cat#78830-5G
tRNA	Roche	Cat#10109495001
Sodium Chloride	Merck	Cat#31434-M
Formamide	Merck	Cat#47671-1L-F
Denhardt's Solution 50x	Merck	Cat#D2532-5X5ML
Ficoll® PM 400	Merck	Cat#F4375-25G
Triton® X-100 for molecular biology	Merck	Cat#T8787-100ML

(*Continued on next page*)

Continued

REAGENT or RESOURCE	SOURCE	IDENTIFIER
Dimethyl sulfoxide	Merck	Cat#D4540-1L
SSPE buffer 20X concentrate	Merck	Cat#S2015-1L
Deoxyribonucleic acid, single stranded from salmon testes	Merck	Cat#D7656-5X1ML
Yeast nitrogen base with amino acids	Merck	Cat#Y1250-250G
Hydrochloric acid	Merck	Cat#30721-1L-M
Ethanol absolute	Merck	Cat#02860-2.5L
Ammonium persulfate	Merck	Cat#A3678-25G
IGEPAL® CA-630	Merck	Cat#I8896-100ML
N,N,N′,N′-Tetramethylethylenediamine	Merck	Cat#T9281-50ML
Dextran sulfate sodium salt from *Leuconostoc spp*	Merck	Cat#D8906-100G
Lithium chloride	Merck	Cat#L9650-100G
Sodium deoxycholate	Merck	Cat#30970-100G
Acrylamide 4X solution	Serva	Cat#10677.1
N,N′-Methylene-bisacrylamide 2X	Serva	Cat#29197.01
2-Propanol	Merck	Cat#I9516-500ML
Glycine for electrophoresis, ≥ 99%	Merck	Cat#G8898-1KG
Formaldehyde solution for molecular biology, 36.5-38% in H2O	Merck	Cat#F8775-500ML
Sodium hydroxide	Merck	Cat#1064621000
Sodium dodecyl sulfate	Merck	Cat#L3771-500G
Trizma® base	Merck	Cat#33742-2KG
Ponceau s sodium practical grade	Merck	Cat#P3504-100G
D-Sorbitol	Merck	Cat#S7547-1KG
Complete Mini	Roche	Cat#11836153001
Ethylenediaminetetraacetic acid ≥ 98.0%	Merck	Cat#03620-1KG
HEPES	Merck	Cat#H4034-1KG
DL-Dithiothreitol	Merck	Cat#43819-25G
Potassium chloride	Merck	Cat#P3911
Sodium phosphate dibasic	Merck	Cat#S9763
Potassium phosphate monobasic	Merck	Cat#P0662
Clarity Western ECL Substrate	Bio-Rad	Cat#1705061
Imidazole	Acros Organics	Cat#396741000
Guanidine hydrochloride	Merck	Cat#G4505-500G
Copper(II) sulfate pentahydrate	Merck	Cat# C8027-500G
Ni-NTA Agarose	QIAGEN	Cat#30210
Critical commercial assays		
Riboprobe System-T7	Promega	Cat#P1440
DECAprime™ II DNA Labeling Kit	Invitrogen	Cat# AM1456
QIAGEN QIAquick PCR Purification Kit	QIAGEN	Cat#28106
QIAquick Gel Extraction Kit	QIAGEN	Cat#28704
QIAprep Spin Miniprep Kit	QIAGEN	Cat#27104
Aurum™ Total RNA Mini Kit	Bio-Rad	Cat#7326820
iScript™ Reverse Transcription Supermix, 100 Rxns	Bio-Rad	Cat#1708841
SsoFast EvaGreen Supermix, 500 Rxns	Bio-Rad	Cat#1725201
Experimental models: organisms/strains		
S. cerevisiae, see Table S1	This paper	N/A

(*Continued on next page*)

Continued

REAGENT or RESOURCE	SOURCE	IDENTIFIER
Oligonucleotides		
ARO+: TGAGTCGTTACAAGGTGATGCC	This paper	N/A
ARO-: ACCTACAGGAGGACCCGAAA	This paper	N/A
DSB 0.2+(ChIP): TCAGACTCAAGCAAACAATCAA	This paper	N/A
DSB 0.2-(ChIP): CCCGTATAGCCAATTCGTTC	This paper	N/A
DSB 0.6+(ChIP): CACCCAAGAAGGCGAATAAG	This paper	N/A
DSB 0.6-(ChIP): CATGCGGTTCACATGACTTT	This paper	N/A
DSB 0.15+(resection): CCTGGTTTTGGTTTTGTAGAGTGG	This paper	N/A
DSB 0.15-(resection): GAGCAAGACGATGGGGAGTTTC	This paper	N/A
DSB 0.65+(resection): GGAAACACCAAGGGAGAG	This paper	N/A
DSB 0.65-(resection): TCTTATTCGCCTTCTTGGGT	This paper	N/A
DSB 0.9+(resection): CGATATTAAGTCCTCCGT	This paper	N/A
DSB 0.9-(resection): CGGCATATTTGTATTAACCC	This paper	N/A
KCC4+: TCGTATCAGGTCTGCCCTATGAA	This paper	N/A
KCC4-: CTCTGGAAATTTCGGTGTCATTG	This paper	N/A
HO CUT+: GTGGCATTACTCCACTTCAA	This paper	N/A
HO CUT-: TCACCACGTACTTCAGCATA	This paper	N/A
EXO1+: GACAAGCGGAAGACAAACTGAC	This paper	N/A
EXO1-: TCCACAACAGTCATGGAGGG	This paper	N/A
DNA2+: GAGTAGGCATCACGATTTCAC	This paper	N/A
DNA2-: GTAGTCATCAGAGTATTCGGCA	This paper	N/A
ALG9+: CCAGGTGATTTTCCAGAGAG	This paper	N/A
ALG9-: GGCCACTCTTTACCGGTATC	This paper	N/A
Software and algorithms		
Bio-Rad CFX Maestro 1.1 Version: 4.1.2433.1219	Bio-Rad	N/A
Image Lab Version 5.2.1	Bio-Rad	N/A
Scion Image Beta 4.0.2	Scion Corporation	N/A
Other		
Primo® FrameStar® 96well PCR Plate, semi-skirted, clear wells	Euroclone	Cat#ECPCR0770C
HYBOND-NX Nylon membrane	GE Healthcare	Cat#GEHRPN203T
Nitrocellulose blotting membrane, Amersham™ Protran™ 0.45 µm NC	GE Healthcare	Cat#GEH10600002
Hyperfilm MP	GE Healthcare	Cat#GEH28906844

RESOURCE AVAILABILITY

Lead contact

Further information and requests for resources and reagents should be directed to and will be fulfilled by the Lead Contact, Maria Pia Longhese (mariapia.longhese@unimib.it).

Materials availability

All unique/stable reagents generated in this study are available from the lead contact without restriction.

Data and code availability

- All data reported in this paper will be shared by the lead contact upon request.
- This paper does not report original datasets or code.
- Any additional information required to reanalyze the data reported in this paper is available from the lead contact upon request.

EXPERIMENTAL MODEL AND STUDY PARTICIPANT DETAILS

Saccharomyces cerevisiae is the experimental model used in this study. Strain genotypes are listed in Table S1. Strains JKM139, used to detect DSB resection and to perform ChIP analyses, and YMV45, used to detect SSA, were kindly provided by J. Haber (Brandeis University, Waltham, USA). The plasmid expressing 6xHis-tagged ubiquitin (2μ *CUP1-6HIS-UBI4*) was kindly provided by R. Fraschini (University of Milan-Bicocca, Milan, Italy).[81] Gene disruptions and tag fusions were generated by one-step PCR and standard yeast transformation procedures. Cells were grown in YEP medium (1% yeast extract, 2% bactopeptone) supplemented with 2% glucose (YEPD), 2% raffinose (YEPR) or 2% raffinose and 3% galactose (YEPRG). All the experiments were performed at 25°C. YEPD plates for *dna2-1* cells also contain sorbitol (0.5M).

METHOD DETAILS

Search for suppressors of *sae2*Δ sensitivity to CPT

To search for suppressor mutations of the CPT sensitivity of *sae2*Δ *rif2*Δ mutant, 5 x 10^6 *sae2*Δ *rif2*Δ cells were plated on YEPD in the presence of 25 μM CPT. Survivors were recovered and crossed to *rif2*Δ cells to identify by tetrad analysis the suppression events that were due to single-gene mutations. The suppressor genes were identified by genome sequencing. To confirm that a mutation was responsible for the suppression, a *URA3* or a *TRP1* gene was integrated downstream of the stop codon and the resulting strain was crossed to wild-type cells to verify by tetrad dissection that the suppression of the *sae2*Δ *rif2*Δ CPT sensitivity co-segregated with the *URA3* or the *TRP1* gene.

DSB repair by single-strand annealing (SSA) and DSB resection at the *MAT* locus

DSB repair by SSA in YMV45 derivative strains was detected by Southern blot analysis using part of the *LEU2* gene as a probe. Quantitative analysis of the repair product was determined by calculating the ratio of band intensities for SSA to the total amount of SSA and DSB products for each time point. DSB resection at the *MAT* locus in JKM139 derivative strains was analyzed on alkaline agarose gels, by using a single-stranded probe complementary to the unresected DSB strand, as previously described.[82] Quantitative analysis of DSB resection was performed by calculating the ratio of band intensities for ssDNA to total amount of DSB products. The resection efficiency was normalized with respect to the HO cleavage efficiency for each time point. Densitometric analysis of band intensities was performed using Scion Image Beta 4.0.2 software. Quantitative PCR (qPCR) analysis of DSB resection at the *MAT* locus in JKM139 derivative strains was carried out as previously described.[83] Briefly, genomic DNA was extracted at different time points following HO induction and digested with both *Ssp*I and *Rsa*I restriction enzymes. A mock reaction without the restriction enzymes was set up in parallel. qPCR was performed on both digested and mock samples with oligonucleotides that anneal at specific distances from the DSB and using SsoFast EvaGreen supermix (Bio-Rad) on the Bio-Rad CFX Connect Real-Time System apparatus. For each time point, Ct values were normalized to those obtained from the mock sample, and then further normalized to values obtained from an amplicon in the *KCC4* control gene. The obtained values were normalized to the HO-cut efficiency measured by qPCR by using oligonucleotides that anneal on opposite sides with respect to the HO-cutting sequence. The percentage of HO-cut was calculated by comparing the Ct values before and after HO induction in undigested samples.

Chromatin immunoprecipitation and qPCR

ChIP analysis was performed as previously described.[84] Quantification of immunoprecipitated DNA was achieved by qPCR on a Bio-Rad CFX Connect Real-Time System apparatus and Bio-Rad CFX Maestro 1.1 software. Triplicate samples in 20 μL reaction mixture containing 10 ng of template DNA, 300nM for each primer, 2x SsoFast EvaGreen supermix (Bio-Rad #1725201) (2x reaction buffer with dNTPs, Sso7d-fusion polymerase, $MgCl_2$, EvaGreen dye, and stabilizers) were run in white 96-well PCR plates Multiplate (Bio-Rad #MLL9651). The qPCR program was as follows: step 1, 98°C for 2 min; step 2, 90°C for 5 s; step 3, 60°C for 15 s; step 4, return to step 2 and repeat 45 times. At the end of the cycling program, a melting program (from 65°C to 95°C with a 0.5°C increment every 5 s) was run to test the specificity of each qPCR. Data are expressed as fold enrichment at the HO-induced DSB over that at the non-cleaved *ARO1* locus, after normalization of each ChIP signal to the corresponding input for each time point. Fold enrichment was then normalized to the efficiency of DSB induction.

Protein extract preparation and western blotting

Protein extracts for western blot analysis were prepared by trichloroacetic acid (TCA) precipitation. Frozen cell pellets were resuspended in 100 μL 20% TCA. After the addition of acid-washed glass beads, the samples were vortexed for 10 min. The beads were washed with 400 μL of 5% TCA, and the extract was collected in a new tube. The crude extract was precipitated by centrifugation at 3000 rpm for 10 min. TCA was discarded and samples were resuspended in 70 μL 2X Laemmli buffer (60mM Tris, pH 6.8, 2% SDS, 10% glycerol, 100mM DTT, 0.2% bromophenol blue), neutralized with 30 μL 1M Tris (pH 8.0). Prior to loading, samples were boiled and centrifuged at 3000 rpm for 10 min. Supernatants containing the solubilized proteins were separated on 10% polyacrylamide gels. Rad51 and Pgk1 were detected by using anti-Rad51 polyclonal antibodies (Ab63798) from Abcam and anti-Pgk1 polyclonal antibodies. HA- and Myc-tagged proteins were detected by using an anti-HA (12CA5) or an anti-Myc (9E10) antibody, respectively. Images were collected using the ChemiDoc (Bio-Rad) and ImageLab software.

Quantitative reverse transcriptase PCR (qRT-PCR)

Total RNA was prepared with the Bio-Rad Aurum total RNA mini kit. First strand cDNA was synthetized with the Bio-Rad iScript™ cDNA Synthesis Kit. After qRT-PCR on a MiniOpticon Real-time PCR system (Bio-Rad), *EXO1* and *DNA2* RNA levels were quantified using the ΔΔCt method and normalized to *ALG9* RNA levels as previously described.[78]

Detection of ubiquitin conjugates

Cells carrying a multicopy plasmid expressing 6xHis-tagged ubiquitin (2μ *CUP1-6HIS-UBI4*) from the copper-inducible *CUP1* promoter were grown to log phase at 25°C in a selective medium. 6xHis-Ubi was induced in half of the culture by the addition of 250 μM $CuSO_4$ for 3 h. Cells were then harvested by centrifugation, resuspended in 10% TCA and lysed by mechanical shearing with glass beads. TCA precipitates were resuspended in buffer A (6 M guanidium-HCl, 100 mM NaCl, 100 mM $NaPO_4$ pH 8, 20 mM Tris-Cl pH 8) with shaking for at least 1 h, and the debris was removed by centrifugation at 2000g. Lysates were incubated overnight at room temperature with Ni-NTA agarose beads (Qiagen, Valencia, CA) in the presence of 10 mM imidazole and 0.1% Triton X-100. Beads were then washed twice with buffer A supplemented with 0.1% Triton X-100 and four times with a wash buffer (100mM NaCl, 100 mM $NaPO_4$ pH 8, 20 mM Tris-Cl pH 8, 10 mM imidazole). Bound proteins were eluted by the addition of 15 μl of elution buffer (100mM NaCl, 100 mM $NaPO_4$ pH 8, 20 mM Tris-Cl pH 8, 500 mM imidazole) and 15 μL of 2X Laemmli buffer (60mM Tris, pH 6.8, 2% SDS, 10% glycerol, 100mM DTT, 0.2% bromophenol blue) before heating 5 min at 95°C. The extracts were then subjected to SDS-PAGE on 10% polyacrylamide gels followed by western blot analysis.

QUANTIFICATION AND STATISTICAL ANALYSIS

Data are expressed as mean values ± standard deviation. Statistical analyses were performed using Microsoft Excel Professional 365 software. *p* values were determined by using an unpaired two-tailed *t*-test. No statistical methods or criteria were used to estimate sample size or to include or exclude samples.